Abdominal Radiology

Published online: 22 February 2018

Abdom Radiol (2018) 43:2309–2320
https://doi.org/10.1007/s00261-018-1480-9

Adding ancillary features to enhancement patterns of hepatocellular carcinoma on gadoxetic acid-enhanced magnetic resonance imaging improves diagnostic performance

Ji Hye Min,[1,2] Young Kon Kim,[1] Dong Hyun Sinn,[3] Seo-Youn Choi,[4] Woo Kyoung Jeong,[1] Won Jae Lee,[1] Sang Yun Ha,[5] Soohyun Ahn,[6] Min-Ji Kim[6]

[1]Department of Radiology and Center for Imaging Science, Samsung Medical Center, Sungkyunkwan University School of Medicine, 81 Ilwon-Ro, Gangnam-gu, Seoul, Republic of Korea
[2]*Present address:* Department of Radiology, Chungnam National University Hospital, Chungnam National University College of Medicine, Daejeon, Korea
[3]Department of Medicine, Samsung Medical Center, Sungkyunkwan University School of Medicine, Seoul, Republic of Korea
[4]Department of Radiology, Soonchunhyang University College of Medicine, Bucheon Hospital, Bucheon, Republic of Korea
[5]Department of Pathology, Samsung Medical Center, Sungkyunkwan University School of Medicine, Seoul, Republic of Korea
[6]Biostatics and Clinical Epidemiology Center, Research Institute for Future Medicine, Samsung Medical Center, Seoul, Republic of Korea

Abstract

Purpose: To assess the added value of intratumoral ancillary features to conventional enhancement pattern-based diagnosis of hepatocellular carcinoma (HCC) on gadoxetic acid-enhanced magnetic resonance imaging (MRI).

Materials and methods: A total of 773 consecutive patients with surgically resected 773 primary hepatic tumors (699 HCCs, 63 intrahepatic cholangiocarcinomas, and 11 benign nodules) who underwent gadoxetic acid-enhanced MRI were retrospectively identified. Enhancement patterns and three ancillary features of capsule, septum, and T2 spotty hyperintensity were assessed by two radiologists. Performance of enhancement pattern-based diagnosis of HCC was compared to diagnosis of HCC based on enhancement pattern plus ancillary features.

Results: Enhancement patterns were positive (arterial diffuse hyperenhancement with washout) for 562 (72.7%) tumors, negative (no arterial hyperenhancement and no washout) for 75 (9.7%), and inconclusive (either no arterial hyperenhancement or no washout) for 136 (17.6%). Capsule was observed in 498 (64.4%) tumors, septum in 521 (67.3%), and T2 spotty hyperintensity in 107 (13.8%). The accuracy and sensitivity of HCC diagnosis was improved significantly after adding at least one ancillary feature compared with enhancement pattern-based diagnosis of HCCs (79.9% vs. 91.1% for accuracy, $p < 0.0001$ and 79.1% vs. 92.0% for sensitivity, $p < 0.0001$) with a minor tradeoff in specificity (87.8% vs. 82.4%, $p = 0.125$). Adding at least two ancillary features improved accuracy (88.1%, $p < 0.0001$) and sensitivity (88.1%, $p < 0.0001$) without changing specificity (87.8%, $p = 1.0$).

Conclusion: Adding intratumoral ancillary features of capsule, septum and T2 spotty hyperintensity to conventional enhancement patterns on gadoxetic acid-enhanced MRI improved accuracy and sensitivity, while maintaining specificity for HCC diagnosis.

Electronic supplementary material The online version of this article (doi:https://doi.org/10.1007/s00261-018-1480-9) contains supplementary material, which is available to authorized users.

Correspondence to: Young Kon Kim; *email:* jmyr@dreamwiz.com

Key words: Hepatocellular carcinoma—Magnetic resonance imaging—Diagnosis—Enhancement—Ancillary feature

Abbreviations

HCC	Hepatocellular carcinoma
MRI	Magnetic resonance imaging
EASL	European Association for the Study of the Liver
AASLD	American Association for the Study of Liver Diseases
CT	Computed tomography
HBP	Hepatobiliary phase
ECCM	Extracellular contrast media
LI-RADS	The liver imaging reporting and data system
IMCC	Intrahepatic mass-forming cholangiocarcinoma
SI	Signal intensity
T1WI	T1-weighted image
T2WI	T2-weighted image
PPV	Positive predictive value
NPV	Negative predictive value

Hepatocellular carcinoma (HCC) can be diagnosed radiologically, without the need for biopsy, if typical imaging features are present [1]. Imaging criteria for HCC diagnosis used by the European Association for the Study of the Liver (EASL) and the American Association for the Study of Liver Diseases (AASLD) are arterial hypervascularization and washout on portal venous and/or delayed phase on four-phase computed tomography (CT) and/or dynamic magnetic resonance imaging (MRI) [1, 2]. As validated in extensive studies in Europe and North America, these criteria give much weight on high specificity of near 100% to avoid false positives rather than offering high sensitivity for HCC diagnosis [3]. However, the typical arterial hypervascularity of HCC may not be shown in many instances, particularly in nodules of 1–2 cm [4].

Gadoxetic acid (Gd-EOB-DTPA; Primovist, Bayer HealthCare, Berlin, Germany), a hepatobiliary MR contrast agent for liver imaging, has received considerable attention due to its capability to delineate HCC as hypointense on hepatobiliary phase (HBP) images [5]. Given that small HCCs often manifest as arterial hyperenhancing nodules without washout on dynamic CT or MRI [6], HBP images have the potential to improve sensitivity for HCC diagnosis. This potential has been demonstrated by a meta-analysis that showed better per-lesion sensitivity of gadoxetic acid-enhanced MRI than extracellular contrast media (ECCM)-enhanced MRI (87% vs. 74%, $p = 0.03$) [7]. In addition, recent meta-analysis has demonstrated superior sensitivity of gadoxetic acid-enhanced MRI than ECCM MRI for detection of small HCCs [8]. Thus, gadoxetic acid-enhanced MRI has been introduced for HCC imaging criteria by the Japan Society of Hepatology [9], the Korean Liver Cancer Study Group [10] and the Liver Imaging Reporting and Data System (LI-RADS) released by the American College of Radiology (http://www.acr.org/Quality-Safety/Resources/LIRADS). However, specificity is controversial because using hypointensity on 3-min delayed phase or HBP images of gadoxetic acid MRI rather than washout on imaging using ECCM might lead to high false positive rates as gadoxetic acid begins to be taken up by hepatocytes approximately 60–90 s after contrast injection. Therefore, hypervascular non-HCC tumors such as small intrahepatic mass-forming cholangiocarcinomas (IMCCs) might be misdiagnosed as HCCs [11].

Because of limitations of current HCC diagnostic criteria, the 2014 version of LI-RADS incorporates a variety of imaging features for tumors itself and outside of tumors (e.g., biliary dilatation) that favor IMCC over HCC (and vice versa) [12]. However, the many imaging features listed make application in real practice difficult, particularly for tumors with multiple conflicting imaging features. In our study, we chose three intratumoral ancillary features: capsule, septum, and T2 spotty hyperintensity, which represent both macroscopic and microscopic pathomorphologic characteristics of HCC with expansive tumor growth [13–15]. We focused on the facts that these features are rarely observed in other hepatic tumors including IMCCs [16]. Therefore, these are helpful for differentiating HCCs from IMCCs.

In this study, we aimed to assess the added value of these ancillary features to conventional enhancement pattern-based diagnosis of HCC on gadoxetic acid-enhanced MRI.

Materials and methods

Study design, setting, participants

This was a retrospective, cross-sectional analysis of patients with available pathology information for primary hepatic tumor and had gadoxetic acid-enhanced liver MRI within 1 months prior to surgery. We screened 2592 consecutive, treatment-naïve patients who underwent gadoxetic acid-enhanced liver MRI for evaluation of primary hepatic tumors between August 2012 and November 2015 at Samsung Medical Center using a computerized search of the hospital system. We included 798 patients who underwent surgery (771 with liver resection and 27 with liver transplantation) as a first-line treatment. For the detailed radiologic-pathologic correlation for ancillary features, 1794 patients with only biopsy results or no pathologic diagnosis were excluded. Twenty-five patients were excluded for a final pathological diagnosis of combined hepatocellular and cholangiocarcinoma in 5 patients

(due to ambiguous imaging features, and inconsistent application of histopathologic criteria) and poor image quality of MRI in 20 patients. Thus, 773 patients (694 with single tumor and 79 with multiple tumors) were analyzed. For the 79 with multiple tumors, we selected a representative index tumor (the largest tumor) for analysis (Fig. 1). The median time interval between MRI and surgical resection was 0.6 months (range 0.1–1.0 months). The institutional review board of Samsung Medical Center approved this retrospective study and waived the requirement for informed consent.

MRI acquisition

MRI was acquired using a 3T MR system (Intera Achieva 3.0 T; Philips Healthcare, Best, the Netherlands) equipped with a dual-source parallel radiofrequency transmission system and quadrature body coil. Baseline MRI included T1-weighted turbo field echo in-phase and opposed sequence (repetition time [TR]/first echo time [TE], second TE, 3.5 ms/1.13 ms [in-phase], 2.3 ms [opposed-phase]; flip angle, 10°; matrix size, 256 × 194; bandwidth, 1785.7 Hz/pixel), a breath-hold multishot T2-weighted sequence with acceleration factor 2 (1796/70; flip angle, 90°; matrix size, 324 × 235; bandwidth, 258.4 Hz/pixel), and a respiratory-triggered single-shot heavily T2-weighted sequence with acceleration factor 2 (1802/160; flip angle, 90°; matrix size, 252 × 254; bandwidth, 420.9 Hz/pixel) with 5 mm section thickness and field of view 32–38 cm. Gadoxetic acid-enhanced imaging consisted of unenhanced, arterial phase (20–35 s), portal phase (60 s), 3-min delayed phase, and 20-min

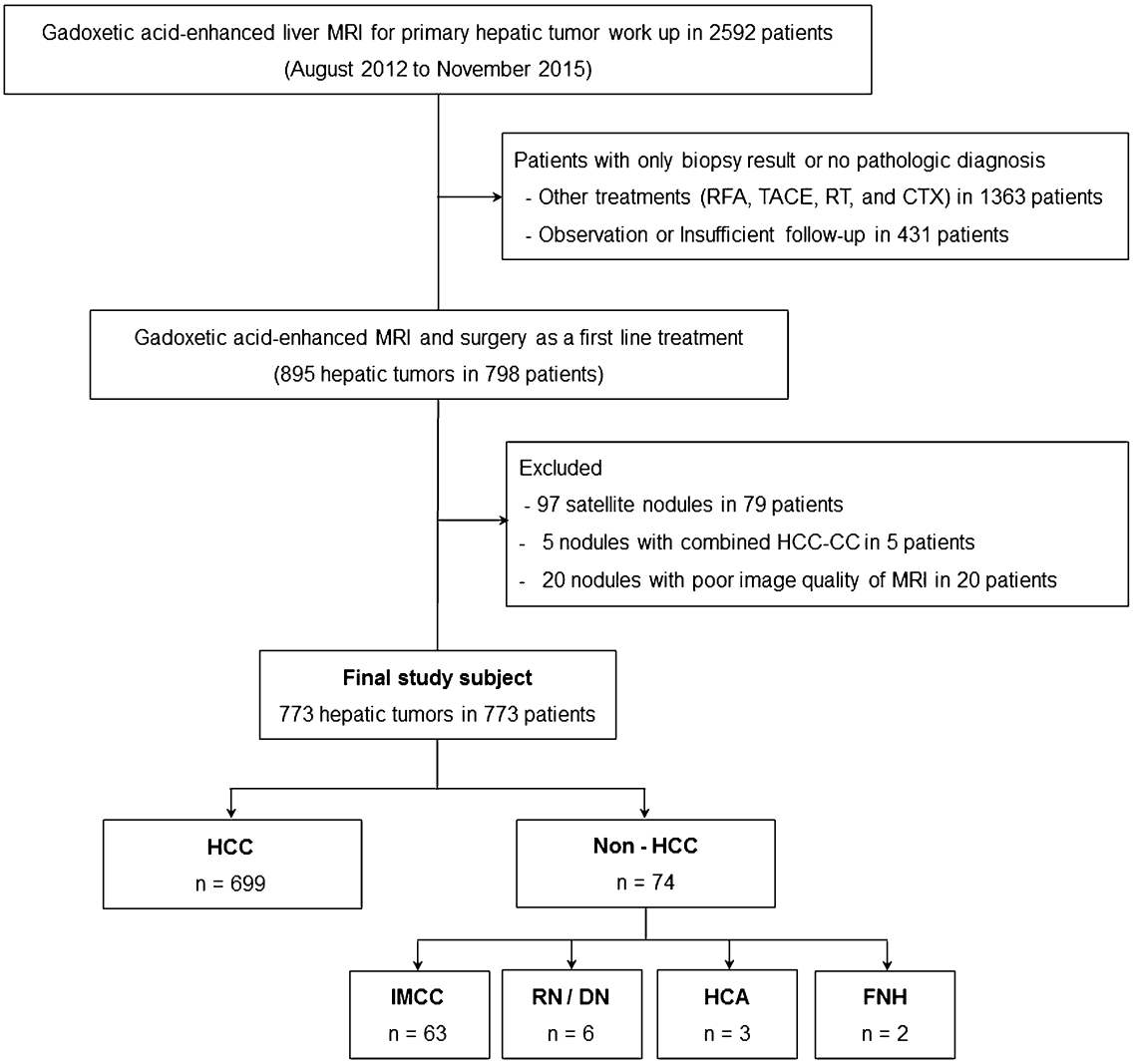

Fig. 1. Flowchart of the study population. MRI, magnetic resonance imaging; RFA, radiofrequency ablation; TACE, transarterial chemoembolization; RT, radiation therapy; CTX, chemotherapy; combined HCC-CC, combined hepatocellular and cholangiocarcinoma; HCC, hepatocellular carcinoma; IMCC, intrahepatic mass-forming cholangiocarcinoma; DN, dysplastic nodule; HCA, hepatocellular adenoma; FNH, focal nodular hyperplasia.

Table 1. MRI sequences and parameters

Sequence	TR/TE (msec)	FA	Section thickness	Matrix size	Bandwidth (Hz/pixel)	Field of view (cm)	Acquisition time (sec)	No. of excitation
T1 W- 3D dual GRE	3.5/1.15–2.3	10°	6 mm	256 × 194	1918.6/0.226	32–38	14	1
BH-MS-T2WI	1623/70	90°	5 mm	324 × 235	255.3/1.702	32–38	55	1
RT-SSH-HT2WI	1156/160	90°	5 mm	376 × 270	388.9/1.117	32–38	120	2
T1 W-3D GRE	3.1/1.5	10°	2 mm	256 × 256	723.4/0.601	32–38	16.6	1
DWI	1600/70	90°	5 mm	112 × 112	79.5/5.467	32–38	126	2

TR/TE, repetition time/echo time; FA, flip angle; GRE, gradient echo; BH-MS-T2WI, breath-hold multishot T2-weighted image; RT-SSH-T2WI, respiratory-triggered single-shot heavily T2-weighted image; DWI, diffusion-weighted image

HBP images obtained using a T1-weighted three-dimensional turbo field echo sequence (enhanced T1 high-resolution isotropic volume examination; eTHRIVE, Philips Healthcare) (TR/TE, 3.1 ms/1.5 ms; flip angle, 10°; matrix size, 256x256; bandwidth, 724.1 Hz/pixel; 2 mm section thickness). Contrast agent was automatically administered intravenously at 1 mL/sec for a dose of 0.025 mmol/kg body weight using a power injector, followed by 20-mL saline flush. The detailed parameters of the MR sequences used are shown in Table 1.

Image analysis

All MRI was evaluated independently by two radiologists (J. H. M. and Y.K.K., with 4 and 16 years of experience in abdominal radiology). Reviewers were blinded to the specific pathological diagnosis of tumors. Before image review, reviewers attended a training session in which the three ancillary features were discussed and illustrated with 30 examples not included in the study. To avoid data clustering from multiple lesions from single patient, a single representative tumor was selected for each patient and marked with an arrow on the image by a radiologist who finalized the study population, but did not participate in the image review (S.Y.C.). In the first analysis session, the reviewers evaluated the imaging patterns of hepatic tumors separately according to enhancement patterns on dynamic phase images and signal intensity (SI) on HBP images. Washout was defined as hypointensity relative to background liver in the portal venous phase according to the LI-RADS v 2014. A total of nine imaging patterns for hepatic tumors on gadoxetic acid MRI were defined based on enhancement pattern on dynamic phase images and SI on HBP images (Table S1). Target appearance in the HBP characterized by central enhancement with a peripheral hypointensity rim [17]. Based on enhancement pattern, the index study (MRI) was positive when a tumor showed arterial diffuse hyperenhancement with washout (type 1 and 2). The index study was negative when the tumor showed no arterial hyperenhancement without washout (types 8 and 9). The index study was inconclusive and considered negative when the tumor showed either arterial diffuse hyperenhancement alone or washout alone (types 3, 4, 5, 6, and 7). After independently evaluating the hepatic tumors with regard to the three categories, the two reviewers then jointly evaluated the enhancement patterns until a consensus was reached, which was used for data analysis. Reviewers also interpreted other features for each hepatic tumor by consensus including presence of lobulated shape, liver surface retraction, biliary obstruction disproportionate to mass diameter, tumor in vein, hyperintense foci on T1-weighted image (T1WI), intralesional fat, target appearance on diffusion-weighted imaging (DWI) [17]. The presence of fat was considered positive when a significant decrease in SI at opposed-phase compared to in-phase images on T1 gradient echo images.

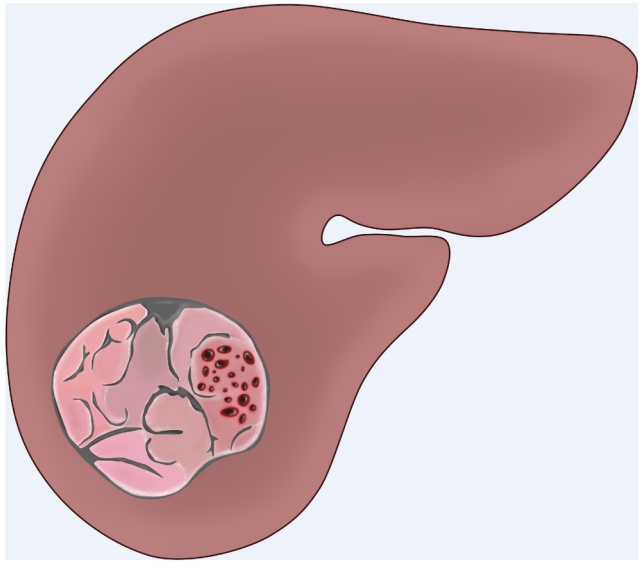

Fig. 2. Illustration of capsule, septum, and T2 spotty hyperintensity of hepatic tumor. Capsule was defined as a peripheral rim around the tumor. Septum was an intratumoral linear structure completely dividing the lesion into more than two compartments. T2 spotty hyperintensity was considered positive when at least three clustered, discrete spotty or tubular hemorrhagic foci were within the hepatic tumor.

In the second session, ancillary features separately evaluated by reviewers were capsule, septum and T2 spotty hyperintensity (Fig. 2). Capsule has been incorporated into major features of HCC in the 2014 version

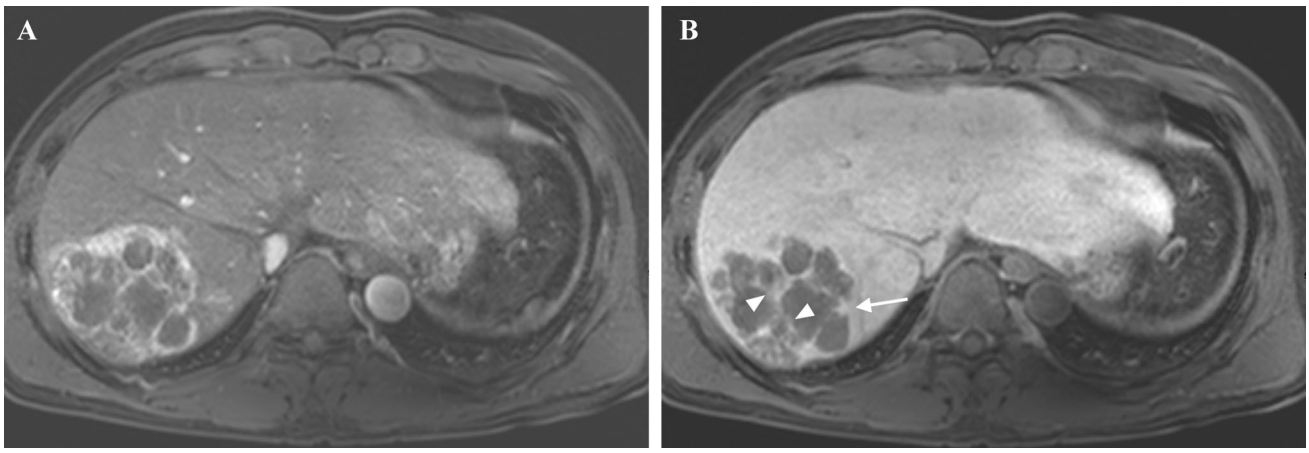

Fig. 3. Hepatocellular carcinoma with an inconclusive enhancement pattern (Type 7), capsule and intratumoral septum on gadoxetic acid-enhanced MRI. The correct diagnosis was reached with the E-plus-A algorithm. Capsule and septum were demonstrated on the pathological specimen. **A** On arterial phase, tumor showed rim enhancement with central hypointensity. **B** On portal venous phase, peripheral rim of smooth hyperenhancement at the margin of tumor (arrow) and intratumoral linear structures (arrowheads) were noted, with washout.

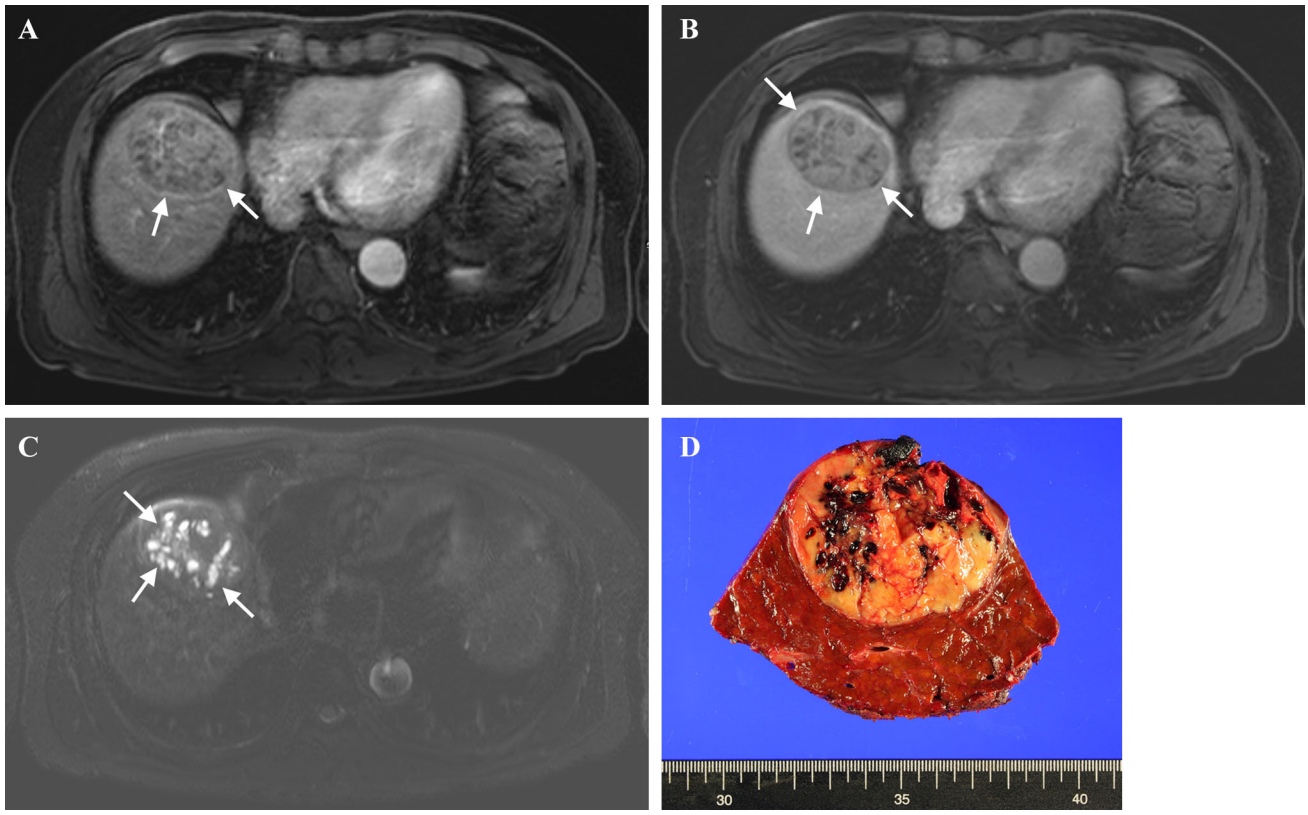

Fig. 4. Hepatocellular carcinoma with an inconclusive enhancement pattern (Type 5), capsule and T2 spotty hyperintensity on gadoxetic acid-enhanced MRI. Use of the E-plus-A algorithm led to a correct HCC diagnosis. Capsule and hemorrhage were demonstrated on the pathological specimen. **A** On arterial phase, tumor showed no definitive arterial hyperenhancement, but showed peripheral rim enhancement with slight internal enhancement (arrows). **B** On portal venous phase, tumor showed slight hypointensity and suspicious peripheral rim with smooth hyperenhancement (arrows). **C** Multiple clustered, discrete, spotty or tubular bright foci within the hepatic tumor observed on the T2-weighted image. **D** Surgical specimen with HCC with multiple hemorrhagic foci.

Table 2. Demographic and pathological characteristics of 773 patients with hepatic tumors

	HCC (n = 699)	Non-HCC (n = 74)	p value
Demographic features			
Age (years)	57.5 ± 10.0*	61.8 ± 10.1*	**<0.001**
Sex			**0.001**
Male	562 (80.4)	50 (67.6)	
Female	137 (19.6)	24 (32.4)	
Underlying liver disease			**<0.001**
Hepatitis B	564 (80.7)	26 (35.1)	
Hepatitis C	53 (7.6)	5 (6.8)	
Others	82 (11.7)	43 (58.1)	
Child–pugh class			0.725
A	584 (83.5)	63 (85.1)	
B	115 (16.5)	11 (14.9)	
No. of cirrhosis	297 (42.5)	23 (31.1)	0.058
AFP	9.9† (1.3–200000)	3.6† (1.3–546.5)	**<0.001**
Gross features on histology			
Size (cm)	3.0† (1.0–20.0)	4.2† (1.0–14.0)	**<0.001**
Size subgroup			**0.007**
<2 cm	148 (21.2)	6 (8.1)	
≥2 cm	551 (78.8)	68 (91.9)	
Fat	137 (19.6)	5 (6.8)	**0.007**
Necrosis	283 (40.5)	45 (60.8)	**0.001**
Hemorrhage	380 (54.4)	2 (2.7)‡	**<0.001**
Microscopic features on histology			
Grade			
I/well	31 (4.4)	2 (3.2)§	
II/moderate	580 (83.0)	35 (55.6)§	
III/poorly	82 (11.7)	26 (41.3)§	
IV	6 (0.9)	–	
Capsule formation‖			**<0.001**
Absence	62 (8.9)	71 (95.9)	
Presence	637 (91.1)	3 (4.1)	
Complete	462 (66.1)	2 (2.7)	
Partial	175 (25.0)	1 (1.4)	
Septum formation¶	574 (82.1)	6 (8.1)	**<0.001**

Bold indicates $p < 0.05$
HCC, hepatocellular carcinoma; AFP, alpha-fetoprotein
Except where indicated, numbers in parentheses are percentages
* Data are presented as mean ± standard deviation
†Data are presented as median (range)
‡In 74 non-HCCs, hemorrhage was detected in 2 hepatocellular adenomas (HCAs)
§Data are from intrahepatic mass-forming cholangiocarcinomas (IMCCs) with well-, moderately, and poorly differentiated adenocarcinomas
‖In 74 non-HCCs, capsule was identified in 1 IMCC and 2 HCAs
¶In 74 non-HCCs, septum was identified in 6 IMCCs

of LI-RADS. However, there is no validated study regarding capsule in gadoxetic acid MRI. Capsule was considered positive when portal venous phase or 3-min delayed phase images demonstrated a peripheral rim of smooth hyperenhancement around the tumor with/without hypointense rim on T1- and T2-weighted images (T2WI) (Figs. 3, 4) [18]. Septum was defined as an intratumoral linear structure that completely divided the lesion into more than two compartments (Fig. 3) [14, 19]. We also regarded as septum when the tumor shows mosaic architecture including the nodule-in-nodule and multi-compartment-in-nodule. The presence of T2 spotty hyperintensity was considered positive when at least three clustered, discrete, spotty or tubular bright foci within the hepatic tumor were observed on T2WI (Fig. 4) [14]. Ancillary features with discrepancies among reviewers after their independent evaluation were re-evaluated to reach a consensus.

Tumor were subdivided into two groups by size: (1) <2 cm and (2) ≥2 cm. Tumor diameter was measured on the axial plane by reviewers using the sequence with the most sharply demarcated margin, avoiding arterial phase, if possible.

Histopathological features

Pathology reports after surgery were the standard of reference. Whole specimens of hepatic masses were retrieved. For HCCs, histopathological factors assessed for each tumor were: nuclear grade, presence of fibrous capsule, septum formation, fat, necrosis or hemorrhage, satellite nodule and multicentric occurrence. Based on

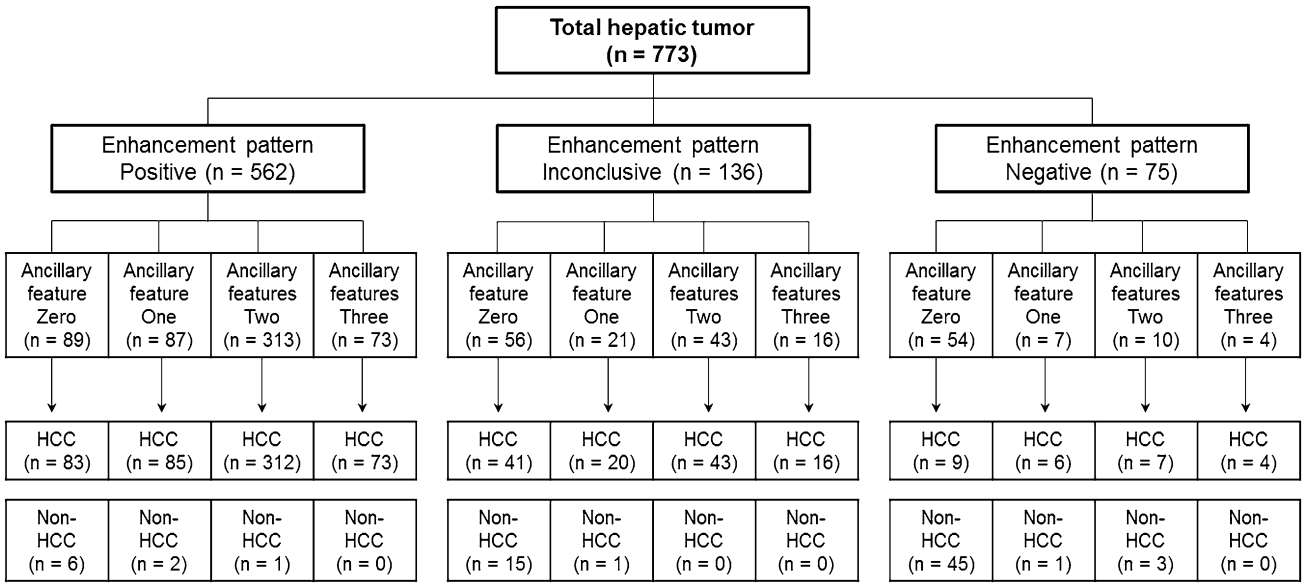

Fig. 5. Diagnostic flow of hepatic tumors according to enhancement pattern and combination of ancillary features on MRI. Based on enhancement pattern, the index study (MRI) was positive when a tumor showed arterial diffuse hyperenhancement with washout (types 1 and 2, Table S1). The index study was negative when the tumor showed no arterial hyperenhancement without washout (types 8 and 9, Table S1). The index study was inconclusive and considered negative when the tumor showed either arterial diffuse hyperenhancement alone or washout alone (type 3, 4, 5, 6, and 7, Table S1).

the nuclear grading scheme proposed by Edmondson and Steiner, HCCs were graded I, II, III, or IV using a basic hematoxylin and eosin stain technique. For tumors with different, coexisting grades, the major part was used for the overall grade. Fibrous capsule formation was recorded as complete (≥90% of tumor circumference), partial (≥50%–90%), or absent (<50%). Intralesional fat was reported as the proportion of area with fatty change to the total cut surface area of resected tumor specimens. For non-HCCs, presence of capsule, septum, hemorrhage, or necrosis was evaluated as for HCCs.

Statistical analysis

Accuracy, sensitivity, specificity, positive predictive value (PPV), and negative predictive value (NPV) for diagnosing HCCs before and after adding ancillary features to conventional enhancement features was evaluated using McNemar's test.

We evaluated the diagnostic performance of each ancillary feature and combination on MRI for HCC diagnosis. Then, we tested the enhancement pattern plus ancillary feature algorithm (E-plus-A algorithm) and assessed diagnostic performance for HCC. For the E-plus-A1 algorithm, the index study was positive if: (1) the tumor showed arterial diffuse hyperenhancement with washout, regardless of ancillary features, (2) the tumor had an inconclusive enhancement pattern, however, at least one ancillary feature was present, (3) the tumor had a negative enhancement pattern, however, with at least two ancillary features. For the E-plus-A2 algorithm, the index study was positive if: (1) the tumor showed arterial diffuse hyperenhancement with washout, regardless of ancillary features, (2) the tumor had an inconclusive enhancement pattern, however, with at least two ancillary features, (3) the tumor had a negative enhancement pattern, however, with all three ancillary features.

Radiologic-pathologic correlation of ancillary features was performed using pathological specimens as reference. For T2 spotty hyperintensity, the presence of hemorrhage on the pathological specimen was the reference based on our pre-analysis correlation between imaging and histology from re-review of specimen including HCC with localized hemorrhagic foci by a pathologist (H.S.Y., 11 years of experience in hepatobiliary disease). Interreviewer agreement for conventional enhancement patterns and ancillary features on MRI was analyzed using kappa statistics with 0.8–1.0 considered agreement that was almost perfect; 0.6–0.79, substantial; 0.40–0.59, moderate; 0.2–0.39, fair; 0–0.19, slight; and 0–1.0, poor [20].

Statistical analyses were performed using SAS version 9.4 (SAS Institute, Cary, NC). A p value less than 0.05 was considered significant.

Results

The final diagnosis of 773 hepatic tumors is summarized in Fig. 1. Patients with HCC were younger, more often

Table 3. Diagnostic performance of gadoxetic acid-enhanced MRI with and without ancillary features for diagnosis of hepatocellular carcinoma

Diagnostic algorithm	Accuracy		Sensitivity		Specificity		PPV (%)	NPV (%)
	(%)	*p* value*	(%)	*p* value*	(%)	*p* value*		
All hepatic tumors (n = 773)								
Enhancement pattern	79.9 (618/773)	–	79.1 (553/699)	–	87.8 (65/74)	–	98.4 (553/562)	30.8 (65/211)
E-plus-A1 algorithm†	91.1 (704/773)	<0.0001	92.0 (643/699)	<0.0001	82.4 (61/74)	0.125	98.0 (643/656)	52.1 (61/117)
E-plus-A2 algorithm†	88.1 (681/773)	<0.0001	88.1 (616/699)	<0.0001	87.8 (65/74)	N/A	98.6 (616/625)	43.9 (65/148)
Hepatic tumors with inconclusive or negative enhancement pattern (n = 211)								
Enhancement pattern	N/A	N/A	N/A	N/A	N/A	N/A	N/A	N/A
E-plus-A1 algorithm†	71.6 (151/211)	N/A	64.6 (90/146)	N/A	93.8 (61/65)	N/A	95.7 (90/94)	52.1 (61/117)
E-plus-A2 algorithm†	60.7 (128/211)	N/A	43.2 (63/146)	N/A	100.0 (65/65)	N/A	100.0 (63/63)	43.9 (65/148)

PPV, positive predictive value; NPV, negative predictive value; N/A, not applicable
* Compared with enhancement pattern-based HCC diagnosis using McNemar's test
†Enhancement pattern plus ancillary feature algorithm (E-plus-A algorithm) was tested assessed for HCC diagnostic performance. For the E-plus-A1 algorithm, the index study was positive if: (1) the tumor showed arterial diffuse hyperenhancement with washout, regardless of ancillary features, (2) the tumor had an inconclusive enhancement pattern, however, at least one ancillary feature was present, (3) the tumor had a negative enhancement pattern, however, with at least two ancillary features. For the E-plus-A2 algorithm, the index study was positive if: (1) the tumor showed arterial diffuse hyperenhancement with washout, regardless of ancillary features, (2) the tumor had an inconclusive enhancement pattern, however, with at least two ancillary features, (3) the tumor had a negative enhancement pattern, however, with all three ancillary features

male, had higher alpha-fetoprotein levels, and more often had hepatitis B as an underlying liver disease. When pathological features were compared to non-HCCs, HCCs were smaller, included fat and hemorrhage and showed capsule and septum formation more often, and showed necrosis less often (Table 2).

Enhancement patterns and other features of hepatic tumors on gadoxetic acid-enhanced MRI

Hepatic tumors were classified into one of nine imaging patterns (Table S1). The enhancement pattern was positive (arterial diffuse hyperenhancement with washout) for 72.7% of hepatic tumors, negative (no arterial hyperenhancement and no washout) for 9.7%, and inconclusive (either no arterial hyperenhancement or no washout) for 17.6% (Fig. 5). HCC was diagnosed for 98.4% of conventional enhancement pattern-positive tumors, 34.7% of negative, and 88.2% of inconclusive tumors. Accuracy, sensitivity, specificity, PPV, and NPV for conventional enhancement pattern-based HCC diagnosis are in Table 3. Overall interreviewer agreement for conventional enhancement patterns with regard to the three categories was substantial for all hepatic tumors (0.70), HCCs (0.61), and non-HCCs (0.75) (Table S2).

As for the other imaging features (Table S1), non-HCCs showed significantly higher frequencies of lobulated shape, liver surface retraction, biliary obstruction disproportionate to mass diameter, and target appearance on DWI. However, HCCs may also present with these features, therefore it is clear that they are not helpful for non-invasive HCC diagnosis. On the other hand, tumor in vein, hyperintense foci on T1WI and intralesional fat were not significantly different.

Diagnostic performance of gadoxetic acid-enhanced MRI with and without ancillary features for HCC diagnosis

Capsule was observed in 498 (64.4%) of tumors, septum in 521 (67.3%), and T2 spotty hyperintensity in 107 (13.8%). Diagnostic performance for each ancillary feature and for combinations is in Table 4. For all hepatic tumors, at least one ancillary feature yielded high accuracy (81.8%), sensitivity (81.0%), and specificity (89.2%). All three ancillary features yielded 100% specificity and PPV with 13.3% sensitivity.

The E-plus-A algorithm improved diagnostic performance compared to conventional enhancement pattern-based HCC diagnosis (Table 3). The E-plus-A1 algorithm (adding at least one ancillary feature) improved accuracy and sensitivity with a minor tradeoff in specificity. The E-plus-A2 algorithm (adding at least two ancillary features) improved accuracy and sensitivity without changing specificity.

The diagnostic performance of ancillary features stratified by enhancement pattern or tumor size is shown in Table S3. It did not significantly differ according to tumors with or without typical HCC enhancement patterns. Ancillary features showed higher accuracy for larger tumors (≥2 cm) than smaller tumors (<2 cm). The E-plus-A algorithm showed improved accuracy and sensitivity regardless of tumor size, with a minor tradeoff or no change in specificity (Table S4).

Table 4. Diagnostic performance of ancillary features on MRI for diagnosis of hepatocellular carcinoma

Ancillary features on MRI	No. of nodules				Diagnostic performance (%)				
	TP	FN	FP	TN	Accuracy	Sensitivity	Specificity	PPV	NPV
All hepatic tumors (n = 773)									
Capsule	493	206	5	69	72.7	70.5	93.2	99.0	25.1
Septum	515	184	6	68	75.4	73.7	91.9	98.8	27.0
T2 spotty hyperintensity	106	593	1	73	23.2	15.2	98.6	99.1	11.0
At least one ancillary feature	566	133	8	66	81.8	81.0	89.2	98.6	33.2
At least two ancillary features	455	244	4	70	67.9	65.1	94.6	99.1	22.3
All three ancillary features	93	606	0	74	21.6	13.3	100.0	100.0	10.9

TP, true positive; FN, false negative; FP, false positive; TN, true negative; PPV, positive predictive value; NPV, negative predictive value

Radiologic-pathologic correlation and interreviewer agreement for ancillary features

Compared with non-HCCs, almost all ancillary features were identified in HCCs on MRI and pathological specimens (Tables 2, 5). For pathological specimens of 699 HCCs, capsule was identified for 637 (91.1%) HCCs, septum for 574 (82.1%), and hemorrhage for 380 (54.4%). For 74 non-HCCs, capsule was identified in 1 IMCC and 2 HCAs. Septum was seen in 6 IMCCs and hemorrhage was detected in 2 HCAs. For pathological specimens by HCC size subgroup, septum and hemorrhage were observed more frequently in HCCs ≥2 cm than HCC <2 cm. However, capsule was more common in HCC <2 cm than in HCCs ≥2 cm (Table S5 and S6).

The radiologic-pathologic correlation for ancillary features is shown in Table 5. For capsule or septum on MRI, sensitivity and PPV were high. Although reviewer sensitivity of T2 spotty hyperintensity was low, PPV was high. By size subgroup, the sensitivity of capsule and septum on MRI was lower in tumors <2 cm, compared with tumors ≥2 cm. T2 spotty hyperintensity on MRI was mostly seen in HCCs ≥2 cm by both reviewers. Sensitivities for T2 spotty hyperintensity were lower in tumors <2 cm, compared with tumors ≥2 cm (Table S5 and S6).

Overall interreviewer agreement for all hepatic tumors was substantial for capsule (0.71), septum (0.78), and almost perfect for T2 spotty hyperintensity (0.85) (Table S7).

Discussion

Compared with current conventional enhancement pattern-based HCC diagnosis, this study found that adding at least one intratumoral ancillary feature of capsule, septum, or T2 spotty hyperintensity to conventional enhancement features (E-plus-A1 algorithm) had significant improvements in accuracy (79.9% vs. 91.1%, $p < 0.0001$) and sensitivity (79.1% vs. 92.0%, $p < 0.0001$) for HCC diagnosis with a minor tradeoff in specificity (87.8% vs. 82.4%, $p = .125$). Addition of at least two ancillary features to enhancement patterns (E-plus-A2 algorithm) improved sensitivity and accuracy without changing specificity. Conventional enhancement criteria showed high specificity (87.8%), but not fully satisfactory sensitivity (79.1%), similar to a previous study [5] using EASL criteria for gadoxetic acid MRI (83.5% sensitivity, 81.2% specificity). In our case series, 40 (5.7%) HCCs showed no arterial hyperenhancement and 80 (11.4%) showed arterial rim enhancement, mimicking IMCCs. Thus, our observations reaffirmed previous reports demonstrating some atypical HCCs including small hypovascular HCCs (≤2 cm) [3] and large HCCs (>5 cm) showing centripetal enhancement pattern [21] or poor arterial enhancement due to a recommended small dose of gadoxetic acid [22] can mimic IMCC. Applying HBP findings can improve sensitivity, but with a tradeoff in specificity, limiting their applicability for non-invasive HCC diagnosis, in particular, in the setting of transplantation in which high specificity is of paramount relevance. The newly suggested E-plus-A algorithm showed significant improvement in sensitivity and accuracy while maintaining high specificity. Thus, E-plus-A algorithm could be beneficial in clinical setting with the emphasis on early detection and early treatment of HCC via surgery or ablation. Our findings indicated that with gadoxetic acid-enhanced MRI, novel HCC diagnostic criteria that do not depend exclusively on conventional enhancement patterns, but use a combination of enhancement patterns plus intratumoral ancillary features improved HCC diagnostic performance.

The internal heterogeneity is fundamental characteristic of HCC [13]. The heterogeneity is attributed to expansive tumor growth that results in capsule and intratumoral septum formation from condensation of fibrous elements of surrounding noncancerous liver tissue (capsule) or tumor tissue with weaker growth compressed by adjacent tumor tissue with more aggressive growth (septum). Capsule or septum is rarely seen in other hepatic tumors; in our study 3 capsules and 6 septa were seen in 74 non-HCCs. HCA is the only other primary liver tumor that can officially have capsule except HCC [23]. Septa can be seen in IMCCs, but abundant fibrous stroma might obscure a fibrous septum. Similar to our study, Qian et al. reported that 4 of 29 IMCCs

Table 5. Radiologic-pathologic correlation for ancillary features using pathological specimens as reference

	HCC (n = 699)			Non-HCC (n = 74)			All (n = 773)		
	Capsule	Septum	T2 spotty hyperintensity*	Capsule	Septum	T2 spotty hyperintensity*	Capsule	Septum	T2 spotty hyperintensity*
Reviewer 1									
Accuracy (%)	71.7 (501/699)	68.4 (478/699)	57.8 (404/699)	86.5 (64/74)	79.7 (59/74)	91.9 (68/74)	73.1 (565/773)	69.5 (537/773)	61.1 (472/773)
Sensitivity (%)	73.2 (466/637)	74.0 (425/574)	25.8 (98/380)	100.0 (3/3)	66.7 (4/6)	0.0 (0/2)	73.3 (469/640)	74.0 (429/580)	25.7 (98/382)
Specificity (%)	56.5 (35/62)	42.4 (53/125)	95.9 (306/319)	85.9 (61/71)	80.9 (55/68)	94.4 (68/72)	72.2 (96/133)	56.0 (108/193)	95.7 (374/391)
PPV (%)	94.5 (466/493)	85.5 (425/497)	88.3 (98/111)	23.1 (3/13)	23.5 (4/17)	0.0 (0/4)	92.7 (469/506)	83.5 (429/514)	85.2 (98/115)
NPV (%)	17.0 (35/206)	26.2 (53/202)	52.0 (306/588)	100.0 (61/61)	96.5 (55/57)	97.1 (68/70)	36.0 (96/267)	41.7 (108/259)	56.8 (374/658)
Reviewer 2									
Accuracy (%)	72.8 (509/699)	72.7 (508/699)	57.9 (405/699)	87.8 (65/74)	82.4 (61/74)	95.9 (71/74)	74.3 (574/773)	73.6 (569/773)	61.6 (476/773)
Sensitivity (%)	73.8 (470/637)	78.2 (449/574)	25.3 (96/380)	66.7 (2/3)	33.3 (2/6)	0.0 (0/2)	73.8 (472/640)	77.8 (451/580)	25.1 (96/382)
Specificity (%)	62.9 (39/62)	47.2 (59/125)	96.9 (309/319)	88.7 (63/71)	86.8 (59/68)	98.6 (71/72)	76.7 (102/133)	61.1 (118/193)	97.2 (380/391)
PPV (%)	95.3 (470/493)	87.2 (449/515)	90.6 (96/106)	20.0 (2/10)	18.2 (2/11)	0.0 (0/1)	93.8 (472/503)	85.7 (451/526)	89.7 (96/107)
NPV (%)	18.9 (39/206)	32.1 (59/184)	52.1 (309/593)	98.4 (63/64)	93.7 (59/63)	97.3 (71/73)	37.8 (102/270)	47.8 (118/247)	57.1 (380/666)

PPV, positive predictive value; NPV, negative predictive value

* For T2 spotty hyperintensity, the presence of hemorrhage on pathological specimens was used as a reference

showed septum-like linear enhancement [16]. Therefore, accurately recognizing capsule and septum on imaging narrows the differential diagnosis for hepatic tumors.

In contrast to other hepatic tumors, multifocal intratumoral septum of HCC might cause multifocal separated areas of hemorrhagic foci that can appear as spotty, bright foci in T2WI. Bright T2WI foci might also be from peliotic changes [14, 24], which are explained by endothelial damage of the sinusoid following increased intratumoral pressure within an encapsulation [24]. This observation could explain the low sensitivity of T2 spotty hyperintensity for histological hemorrhage by both reviewers (25.7% and 25.1%). However, specificity (95.7% and 97.2%) was high, indicating the potency of T2 spotty hyperintensity to characterize large HCCs that commonly accompany hemorrhage and/or necrosis and often show atypical enhancement [21, 22]. In our study, HCCs ≥2 cm showed T2 spotty hyperintensity and hemorrhage more often than smaller HCCs. Similarly, LI-RADS suggests 'blood products' as one of ancillary features favoring HCC; however, no specific imaging features have been demonstrated. Prevalence of capsule, septum and mosaic appearance in HCC is known to correspond to greater tumor size [15, 25]. However, in our study, septum and hemorrhage were observed more frequently in HCCs ≥2 cm than HCC <2 cm, although the prevalence of capsule were similar in both groups. Thus, intratumoral ancillary features help distinguish between relatively large HCCs and other tumors, particularly IMCCs, rather than distinguishing between early HCCs and dysplastic nodules. Overall interreviewer agreement was substantial for capsule (0.71) and septum (0.78), and almost perfect for T2 spotty hyperintensity (0.85). These results revealed a need for improved, objective definitions and imaging technology.

This study has limitations. First, the retrospective study design may have led to biases including selection, measurement or misclassification bias. To define the gold standard for diagnosis, we only included tumors with pathological specimens. This inclusion inevitably introduces selection bias. Thus, the number of non-HCC tumor or cirrhosis-related benign nodule was small. Nevertheless, it reflects real practice. Also, without surgical whole specimens, we could not assess the pathomorphologic feature such as capsule, septum. Radiological images were re-evaluated to minimize measurement bias but pathological specimens were not re-evaluated by a single pathologist. Because of the long study duration, different pathologists evaluated pathological specimens. However, pathologists were unaware of the study aims and used a standardized reporting format for specimens that included information on septum, capsule and hemorrhages. Hence, measurement error in the pathology variables was unlikely to result in severe misclassification bias. Second, since we focused on intratumoral ancillary features that are highly specific for HCC, our methodology did not allow us to consider all ancillary features that favor or not favor HCC as we do in real practice; however, comparison of our algorithm based on three ancillary features to algorithms using all ancillary features or the LI-RADS is beyond the scope of this study. Third, more than half of the patients in non-HCC group had no hepatitis B or C, which is a substantial limitation of the study design.

In conclusion, adding intratumoral ancillary features of capsule, septum, and T2 spotty hyperintensity to conventional enhancement patterns on gadoxetic acid-enhanced MRI-improved accuracy and sensitivity, while maintaining specificity for HCC diagnosis.

Compliance with ethical standards

Conflict of interest No conflict of interest.

References

1. Bruix J, Sherman M, American Association for the Study of Liver D (2011) Management of hepatocellular carcinoma: an update. Hepatology 53:1020–1022. doi:https://doi.org/10.1002/hep.24199
2. European Association For The Study Of The L, European Organisation For R, Treatment Of C (2012) EASL-EORTC clinical practice guidelines: management of hepatocellular carcinoma. J Hepatol 56:908–943. doi:https://doi.org/10.1016/j.jhep.2011.12.001
3. Forner A, Vilana R, Ayuso C, et al. (2008) Diagnosis of hepatic nodules 20 mm or smaller in cirrhosis: prospective validation of the noninvasive diagnostic criteria for hepatocellular carcinoma. Hepatology 47:97–104. doi:https://doi.org/10.1002/hep.21966
4. Bolondi L, Gaiani S, Celli N, et al. (2005) Characterization of small nodules in cirrhosis by assessment of vascularity: the problem of hypovascular hepatocellular carcinoma. Hepatology 42:27–34. doi:https://doi.org/10.1002/hep.20728
5. Choi SH, Byun JH, Lim YS, et al. (2016) Diagnostic criteria for hepatocellular carcinoma 3 cm with hepatocyte-specific contrast-enhanced magnetic resonance imaging. J Hepatol 64:1099–1107. doi:https://doi.org/10.1016/j.jhep.2016.01.018
6. van den Bos IC, Hussain SM, Dwarkasing RS, et al. (2007) MR imaging of hepatocellular carcinoma: relationship between lesion size and imaging findings, including signal intensity and dynamic enhancement patterns. J Magn Reson Imaging 26:1548–1555. doi:https://doi.org/10.1002/jmri.21046
7. Lee YJ, Lee JM, Lee JS, et al. (2015) Hepatocellular carcinoma: diagnostic performance of multidetector CT and MR imaging-a systematic review and meta-analysis. Radiology 275:97–109. doi:https://doi.org/10.1148/radiol.14140690
8. Kierans AS, Kang SK, Rosenkrantz AB (2016) The diagnostic performance of dynamic contrast-enhanced MR imaging for detection of small hepatocellular carcinoma measuring up to 2 cm: a meta-analysis. Radiology 278:82–94. doi:https://doi.org/10.1148/radiol.2015150177
9. Kudo M, Matsui O, Izumi N, et al. (2014) JSH consensus-based clinical practice guidelines for the management of hepatocellular carcinoma: 2014 update by the liver cancer study group of Japan. Liver Cancer 3:458–468. doi:https://doi.org/10.1159/000343875
10. Korean Liver Cancer Study G, National Cancer Center K (2015) 2014 KLCSG-NCC korea practice guideline for the management of hepatocellular carcinoma. Gut Liver 9:267–317. doi:https://doi.org/10.5009/gnl14460
11. Joo I, Lee JM, Lee DH, et al. (2015) Noninvasive diagnosis of hepatocellular carcinoma on gadoxetic acid-enhanced MRI: can hypointensity on the hepatobiliary phase be used as an alternative to washout? Eur Radiol 25:2859–2868. doi:https://doi.org/10.1007/s00330-015-3686-3
12. Mitchell DG, Bruix J, Sherman M, Sirlin CB (2015) LI-RADS (Liver Imaging Reporting and Data System): summary, discussion, and consensus of the LI-RADS Management Working Group and

future directions. Hepatology 61:1056–1065. doi:https://doi.org/10.1002/hep.27304
13. Ishizaki M, Ashida K, Higashi T, et al. (2001) The formation of capsule and septum in human hepatocellular carcinoma. Virchows Arch 438:574–580
14. Kadoya M, Matsui O, Takashima T, Nonomura A (1992) Hepatocellular carcinoma: correlation of MR imaging and histopathologic findings. Radiology 183:819–825. doi:https://doi.org/10.1148/radiology.183.3.1316622
15. Kojiro M, Nakashima T (1987) Pathology of hepatocellular carcinoma. In: Okuda K, Ishak KG (eds) *Neoplasm of the Liver*. Tokyo, Japan: Springer, pp 81–104
16. Qian H, Li S, Ji M, Lin G (2016) MRI characteristics for the differential diagnosis of benign and malignant small solitary hypovascular hepatic nodules. Eur J Gastroenterol Hepatol 28:749–756. doi:https://doi.org/10.1097/MEG.0000000000000642
17. Park HJ, Kim YK, Park MJ, Lee WJ (2013) Small intrahepatic mass-forming cholangiocarcinoma: target sign on diffusion-weighted imaging for differentiation from hepatocellular carcinoma. Abdom Imaging 38:793–801. doi:https://doi.org/10.1007/s00261-012-9943-x
18. Ishigami K, Yoshimitsu K, Nishihara Y, et al. (2009) Hepatocellular carcinoma with a pseudocapsule on gadolinium-enhanced MR images: correlation with histopathologic findings. Radiology 250:435–443. doi:https://doi.org/10.1148/radiol.2501071702
19. Suh YJ, Kim MJ, Choi JY, et al. (2011) Differentiation of hepatic hyperintense lesions seen on gadoxetic acid-enhanced hepatobiliary phase MRI. AJR Am J Roentgenol 197:W44–52. doi:https://doi.org/10.2214/AJR.10.5845
20. Landis JR, Koch GG (1977) The measurement of observer agreement for categorical data. Biometrics 33:159–174
21. Blaschke EM, Rao VL, Xiong L, et al. (2016) Multiphase multidetector row computed tomography imaging characteristics of large (>5 cm) focal hepatocellular carcinoma. J Comput Assist Tomogr 40:493–497. doi:https://doi.org/10.1097/RCT.0000000000000379
22. Kanata N, Yoshikawa T, Ohno Y, et al. (2013) HCC-to-liver contrast on arterial-dominant phase images of EOB-enhanced MRI: comparison with dynamic CT. Magn Reson Imaging 31:17–22. doi:https://doi.org/10.1016/j.mri.2012.06.012
23. Marti-Bonmati L (1997) MR imaging characteristics of hepatic tumors. Eur Radiol 7:249–258. doi:https://doi.org/10.1007/s003300050146
24. Fujimoto M, Nakashima O, Komuta M, et al. (2010) Clinicopathological study of hepatocellular carcinoma with peliotic change. Oncol Lett 1:17–21. doi:https://doi.org/10.3892/ol_00000003
25. Honda H, Onitsuka H, Murakami J, et al. (1992) Characteristic findings of hepatocellular carcinoma: an evaluation with comparative study of US, CT, and MRI. Gastrointest Radiol 17:245–249